Eur. Phys. J. Special Topics **227**, 179–199 (2018)

https://doi.org/10.1140/epjst/e2018-00046-4

THE EUROPEAN PHYSICAL JOURNAL SPECIAL TOPICS

Regular Article

High strain rates testing and constitutive modeling of B500B reinforcing steel at elevated temperatures

Ezio Cadoni[1,a], Mario Fontana[2], Daniele Forni[1], and Markus Knobloch[3]

[1] DynaMat Laboratory – University of Applied Sciences of Southern Switzerland, 6952 Canobbio, Switzerland
[2] Institute of Structural Engineering, ETH Zurich, 8093 Zurich, Switzerland
[3] Institute of Steel, Lightweight and Composite Structures, Ruhr-Universität Bochum, 44801 Bochum, Germany

Received 13 July 2017 / Received in final form 31 December 2017
Published online 10 September 2018

Abstract. Understanding the response of the building materials under extreme condition of loading (blast and impact events) and temperature (fire) is fundamental for civil engineers to design safe structures for civil or defense applications. In this paper an experimental investigation on the influence of the combined effects of high strain rate and elevated temperature on the mechanical properties of B500B reinforcing steel in tension is presented. The quasi-static tensile tests have been performed at temperatures of 20 °C, 200 °C, 400 °C and 600 °C under steady-state conditions at ETH Zurich, using a closed-loop strain rate control system. The mechanical characterization at high strain rate has been performed by means of a Split Hopkinson Tensile Bar installed at the DynaMat Laboratory (SUPSI). In order to evaluate the extreme combined effect of dynamic loadings and elevated temperatures a water-cooled induction heating system was used. The tensile stress-strain response of B500B steel is found to depend strongly on both the applied strain rate and the test temperature. Dynamic tests at room temperature highlight an increase of strength and strain capacities. At high strain rate the increase of the temperature causes a decrease of strength, strain and energy absorbed in the plastic deformation. The strain hardening rate of this material is analysed as a function of strain rate and temperature. Two widely used constitutive laws (Johnson-Cook and Cowper-Symonds) have been calibrated. Numerical and experimental results have been compared. This research provides new data that starts to cover the lack of information about this widely used reinforcing steel in reinforced concrete structures. The degradation factors of different mechanical properties of B500B steel can be used by the designer in case of multi-hazard scenario, such as fire followed by an explosion.

[a] e-mail: ezio.cadoni@supsi.ch

1 Introduction

Nowadays the demand for safety for reinforced concrete structures and critical infrastructures is more and more important for our society. First of all, because the growth of man-made accidents (terroristic attacks) has shown the vulnerability of our built environment; secondly, some infrastructures are subjected to unexpected phenomena due to climate change (rockfalls, hurricanes, floodings); moreover, the progressive collapse of structures caused by fire and/or explosions are increasingly frequent and this highlights a lack of knowledge and consequent inadequacy of robustness of these structures against severe loadings; finally, the accidents in tunnels (causing fire and/or blast), impact and/or fire in the off-shore structures as well as missiles or aircraft impacts on structures continue to be the most critical safety issues (for example in nuclear power plants but not only).

To respond to this safety demand it is fundamental to know the actual response of reinforced concrete structures when subjected to severe accidental loads. In particular, this analysis should be based on the true behaviour of the materials (concrete and rebar) under the same extreme conditions. The best way to study the behaviour of a reinforced structures, for example, subjected to fire and blast loads is the experimental test, that is the real test for all theoretical and numerical predictions. Unfortunately this approach is costly and in many cases not possible because of safety and/or environmental issues. Thanks to the rapid development of modeling and numerical simulation, it is today possible to faithfully predict the dynamic response of reinforced structures subjected to blast/impact loads and fire. But this cannot be achieved without the knowledge of the material behaviour under high strain rate and high temperature. Understanding dynamic strength properties of reinforcing steel subjected to fire, blast or impact loads is then required for structural assessment and design of critical reinforced concrete structures able to withstand to these extreme events.

In a multi-hazard loading scenario of impact-fire is actually necessary to define the dependence of the strength, energy absorption and ductility of the building materials on high strain rate loading and high temperatures. Mirmomeni et al. [1,2] investigated how the damage caused by impact load alters the fire resistance of mild steel from the aspect of mechanical damage. The same multi-hazard approach has been used by Forni et al. [4–6] to study the residual load bearing capacity of steel columns under fire conditions and followed by an explosion starting from an extensive testing campaign in tension in a wide range of strain rate and temperature. These results are of great interest for the assessment of robustness in structures where progressive collapse may be triggered by the failure of parallel steel members. Similar approach can be applied for reinforced concrete structures. Currently, the attention of several researches is still too focused on the dynamic tensile behaviour of concrete and rarely the dynamic behavior of reinforcing steel is considered.

Recently, some experimental studies have been addressed on the mechanical behaviour of reinforcing steel at elevated temperatures [7–10] or at high strain rate [11–16]. It can be noted how information about the combination of strain rate and temperature are practically absent in literature. In order to cover the lack of data on the mechanical properties of reinforcing steel with the coupled effect of elevated temperatures and high strain rates part of the research named *Behaviour of structural steels under fire in a wide range of strain rates* – developed in the frame of the COST Action TU0904 'Integrated Fire Engineering and Response' by the DynaMat Laboratory (SUPSI) and the Institute of Structural Engineering (ETH Zürich) – was dedicated to three reinforcing steels (B500A, B500B and stainless steel AISI304). Preliminary results has been lately published in [3] where a first comparison of the three abovementioned reinforcing steels is shortly presented.

The aim of the present research is to investigate the influence of temperature, high strain rate and their combination on the mechanical behaviour of B500B reinforcing steel in tension by performing dynamic tests under different strain rates ranging from 10^{-3} s^{-1}, 250 s^{-1}, 400 s^{-1} and 800 s^{-1} and at temperatures of 20 °C, 200 °C, 400 °C, 600 °C. These experimental results are used to calibrate the widely used material constitutive relationships (Cowper-Symonds and Johnson-Cook).

2 Outlook on the strain rate and temperature effects on reinforcing steel mechanical properties

2.1 Effects of the strain rate

The strain rate effect on the mechanical behavior of materials is well known even if not yet accurately studied for all materials, specially for construction materials. In metals, it depend on how the local imperfections such as (self- or external) inclusions, vacancies or grain boundaries evolve in function of time when the material is invested by a stress wave; this causes a micro-structural evolution driven by the kinetic of dislocations. Generally, it consists in an enhancement of the tensile strength and a decrease of ductility and/or strain capacity, similar behaviour is obtained decreasing the temperature. In the last decades many researches have studied the strain rate effects on concrete but only few of them have analysed what occur in the reinforcing steel. As reported in a recent review [17] only a limited number of relationships have been proposed in literature.

The effect of strain rate on the strength properties of reinforcing steels is typically represented by the dynamic increase factor (DIF) – that is the ratio between the dynamic and static strength – versus strain rate. A first relation was proposed by Comité Euro-International du Beton [18] and recently recalled in the Model Code 2010 [19].

$$\frac{f_{yd}}{f_{ys}} = 1 + \frac{6.0}{f_{ys}} \ln \frac{\dot{\epsilon}}{\dot{\epsilon}_s}, \tag{1}$$

$$\frac{f_{ud}}{f_{us}} = 1 + \frac{7.0}{f_{us}} \ln \frac{\dot{\epsilon}}{\dot{\epsilon}_s}, \tag{2}$$

where f_{yd} is the dynamic yield stress, f_{ys} is the quasi-static yield stress, f_{ud} is the dynamic ultimate tensile strength, f_{us} is the quasi-static ultimate tensile strength, $\dot{\epsilon}$ is the strain rate. This relation is valid only till a strain rate of 10 s^{-1}, the reference quasi-static strain rate is $\dot{\epsilon}_s = 5 \times 10^{-5}$ s^{-1}.

Another empirical relation was proposed by Malvar [20] as a result of a literature review on the properties of rebars with yield stresses ranging from 290 to 710 MPa. This relation is valid only till a strain rate of 10 s^{-1}.

$$\frac{f_{yd}}{f_{ys}} = \left(\frac{\dot{\epsilon}}{10^{-4}}\right)^{0.074-0.040\frac{f_{ys}}{414}}, \tag{3}$$

$$\frac{f_{ud}}{f_{us}} = \left(\frac{\dot{\epsilon}}{10^{-4}}\right)^{0.019-0.009\frac{f_{ys}}{414}}. \tag{4}$$

These formulae have been included in the Model Code. They have extended the Malvar's formulae to the high strain rate regime, higher than 10 s^{-1} (limit of validity of the Malvar's study). In recent studies it has been demonstrated how the high strain rate regime is not well described by the previous relationships, specially because of lack of experimental data. In the case of B500A reinforcing steel, these formulae can be extended for the ultimate tensile strength but not for the yield stress, in fact the value is overestimated respect the experimental results [21]. In another research the B450C reinforcing steel has been analysed both at experimental [22] and numerical point of view [23]. The ultimate tensile strength obtained by using the Malvar's formula is decisively underestimated. Finally, the high strain rate results obtained from austenitic stainless reinforcing steel [24] indicated that an overestimation of the ultimate tensile strength and an underestimation of yield stress. These experimental results highlight an urgent need for data in this dynamic regime that is fundamental for the design and/or assessment of reinforced concrete structures subject to extreme loads. Several other authors proposed similar descriptions and for brevity these have not been listed.

2.2 Effects of the elevated temperature

The elevated temperature affects the mechanical properties of rebars, because of transformations in the material. The influence of the temperature on the mechanical behaviour of rebars is generally studied with the aim to obtain information on their residual mechanical properties. The residual values of the key parameters, such as modulus of elasticity, yield strength, and ultimate tensile strength, are regularly described in terms of reduction factors. Tao et al. [25] analysed the phenomena that can affect the residual properties as the cooling rate, the cooling method, the preloading. Their tests showed that both the yield strength and ultimate strength are not affected by heating for temperature lower than 500 °C, while for higher temperature a lost of strength is observed. Elghazouli et al. [26] studied the behaviour of hot-rolled and cold-worked reinforcement at ambient and elevated temperature. Aim of this study was to assess the behaviour of small diameter plain and deformed bars usually employed in composite slabs. Through steady-state and transient elevated temperature conditions they analysed the material response, including the residual properties of the rebar after cooling. Felicetti et al. [10] investigated the residual mechanical properties of seven types of reinforcing steel exposed to high temperature. They found that quenched and self-tempered rebars are more sensitive to high temperature than the other carbon-steel bars for temperature above 550 °C. Regarding the response of stainless steels exposed to high temperature, they found a very good behaviour in the case of hot-rolled rebar but a considerable lost of strength in the case of cold-worked bars. These findings reveal how the residual mechanical properties of the rebars subjected to fire loads, when measured after cooling, are of capital importance for a reliable assessment of structural members post-fire with the aim to base the structural rehabilitation on consistent data. Furthermore, the evaluation of the mechanical properties is critical when during a fire a blast (or impact) event occurs.

The knowledge of this behaviour is then an essential information for a multi-hazard analysis on structures. For this reason the combined effects have to be studied to correctly verify the actual safety level of materials and structures.

3 Material: B500B reinforcing steel

The mechanical properties of rebars for concrete structures are prescribed by current standards ([27,28]) that require minimum values for yield stress (f_y), ultimate tensile

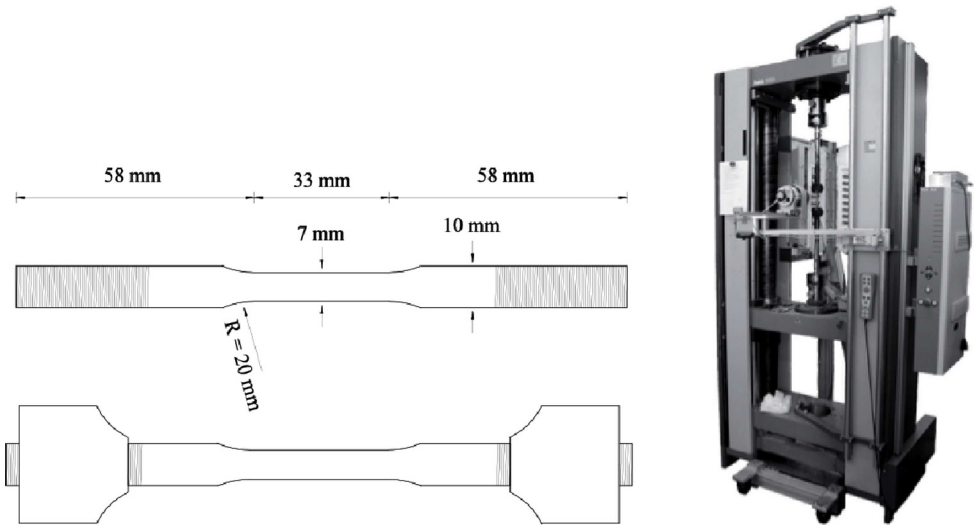

Fig. 1. (a) Geometry of quasi-static tensile test specimens. (b) Set-up for quasi-static test at high temperature.

strength (f_u), elongation to failure (ϵ_u) as well as the hardening ratio f_u/f_y. The hot rolled reinforcing bar B500B is normally adopted as normal ductility ribbed rebar for the reinforced concrete structure. The capital letter B, preceding the nominal yield strength (500 MPa), designates reinforcing steel, while B is the ductility class in accordance with EN 1992-1-1 [29] who defines in terms of the ratio $f_u/f_y \geq 1.08$ and elongation to failure ($A_{gt} \geq 5\%$).

4 Experimental set-up, procedure and specimens for quasi-static tests at elevated temperature

The elevated-temperature quasi-static mechanical properties were examined based on an extensive tensile testing program at various temperatures. Besides reference temperature tests at ambient temperature, the quasi-static tensile tests were performed at temperatures of 200, 400 and 600 °C under steady-state conditions at ETH Zurich, using a closed-loop strain rate control system, to which were fed back strain measurements that were established inside the furnace with a high-precision extensometer directly at the specimen. The tests were performed two times per elevated temperature level with two different constant strain rates of 0.2 (33×10^{-6} s^{-1}) and 1.0%/min (167×10^{-6} s^{-1}). The stress-strain lines of two tests coincided always very well. Figure 1a displays the geometry of the material samples. The nominal diameter of the slender part of the reinforcing steel was 7 mm. The actual dimensions of the test specimens were taken prior to testing. All specimens were equipped on the surface with two K-type thermocouples at the top and bottom part. A combined setup of a split-tube electric furnace and a universal testing machine with a capacity of ±200 kN was used to perform the tensile tests at elevated temperatures. Figure 1b shows a photograph of the universal testing machine and the open furnace with the high-temperature resisting extensometer attached to the specimen. The temperature signals of the two K-type thermocouples were used as feedback variables to control

the lower and upper heating zones of the furnace that features three independently controllable heating zones in vertical direction. The furnace air temperature measured with a type N mantle thermocouple served as feedback variable for the control of the heating zone in the middle. The elongation of the specimen was measured inside the furnace directly on the specimen's surface with the ceramic rods of the extensometer and served as feedback variable of the closed-loop strain rate control system. The force in the specimen was continuously recoded with a load cell of a capacity of 200 kN. The test procedure consisted of three phases. In the first phase, the specimen was built into the machine. The Young's modulus was established with a series of strain rate controlled loading and unloading cycles to check the specimen's axial alignment in the machine. In the second phase, the thermal cycle started. The specimen was heated with a constant rate of 15 K/min to the target temperature. Subsequently, steady-state conditions in the specimen were reached during a conditioning phase of 30 min. In the final phase, the specimen was loaded strain rate controlled beyond the ultimate tensile strength. In addition to the overall stress-strain response, mechanical parameters were obtained from the test results. The elastic modulus was determined as the slope of the initial linear part of the experimental stress-strain line. The proportional limit was determined as the stress level at which the relative deviation of the experimental strain coordinate from the elastic line exceeded 2%. The 0.2%-proof stress was determined with an offset method with an offset value of 0.2% residual strain. The ultimate tensile strength was determined from the coordinates of the peak point of the stress-strain line.

5 Testing set-up, procedure and specimens for high strain rates and elevated temperatures

5.1 Experimental set-up for high strain rates testing

The mechanical properties of materials at high strain rates are usually obtained by means of the Split Hopkinson Bar technique. It generates a well controlled loading pulse in terms of rise time, amplitude and duration, giving rise to the propagation of an uniaxial elastic plane stress wave [22]. Based on the uniaxial elastic stress wave propagation theory developed by [30–32] the method assures accurate measurements and high precision results. In this experiments the Split Hopkinson Tensile Bar (SHTB) developed in the seventies by Albertini et al. [33,34] was used. It consists of two circular steel bars with a diameter of 10 mm, having a length of 9 and 6 m, respectively (see Fig. 2a). The first 6 m of the first bar is used as used as pulse generator and is called *pretensioned bar* ②, the remaining 3 m is used as *input bar* ④ while the second bar acts as *output bar* ⑧. The *round specimen* ⑥ is screwed to the input and output bars. The test is performed as follow: (i) the *blocking device* ③ blocks the pretensioned bar in one end; (ii) the other end is directly connected with a *hydraulic actuator* ①, of maximum loading capacity of 600 kN; (iii) by pulling statically the pretensioned bar is possible to store energy in it; (iv) by rupturing the fragile bolt in the blocking device the system is subject to a tensile mechanical pulse of 2.4 ms duration with linear loading rate during the rise time, propagating along the input and output bars bringing to fracture the specimen. The pulse propagates with the velocity C_0 of the elastic wave with its shape remaining constant. When the incident pulse (ϵ_I) reaches the specimen, part of it (ϵ_R) is reflected by the specimen whereas another part (ϵ_T) passes through the specimen propagating into the output bar. The length of the pretensioned bar and of the output bar is the same (6 m) because for the first it is necessary to generate a long tensile pulse (2.4 ms) ensuring

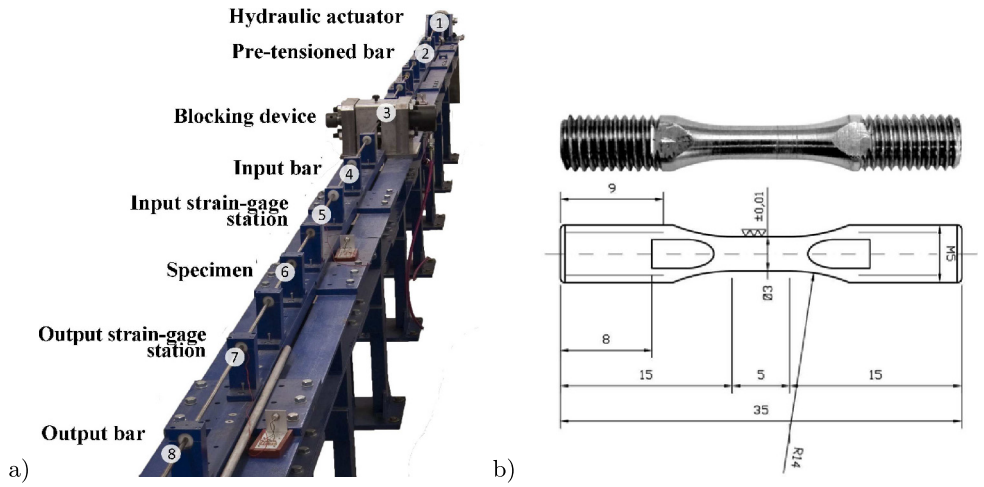

Fig. 2. (a) SHTB for dynamic testing. (b) Geometry of dynamic tensile test specimens.

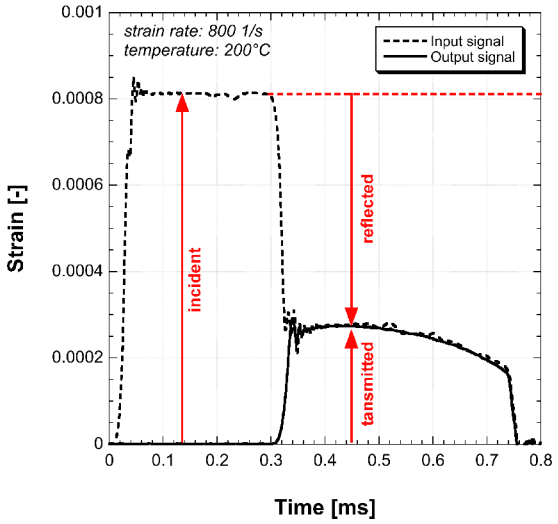

Fig. 3. Incident, reflected and transmitted pulses.

a constant strain rate deformation to the specimen, while for the second this length it is required to allow the specimen deformation avoiding the superposition of the wave reflected from the free end of the output bar. Specimens were obtained by rebars of 12 mm in diameter by turning these bars, obtaining the current geometry, 3 mm in diameter and 5 mm of gauge length, used in dynamic testing with the SHTB is shown in Figure 2b.

The signals from the input and output strain gauges are shown in Figure 3. The input strain gauge ⑤ measures the superposition of the incident and reflected pulse $(\epsilon_I + \epsilon_R)$ while the output strain gauge ⑦ measures the transmitted (ϵ_T) one. It is possible to observe that in the plastic region there is the confirmation of the achievement of force equilibrium within the sample $(\epsilon_I + \epsilon_R = \epsilon_T)$. Because the incident pulse is constant for 2.4 ms the reflected pulse is easily obtained by subtracting the incident pulse (rectangular wave) from the input signal. The premises

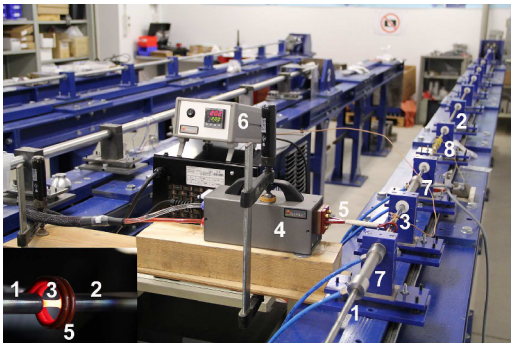

Fig. 4. Experimental set-up for the combination of high strain rate tests and high temperatures.

for the application of the one-dimensional elastic plane stress wave propagation theory are verified [21,22], and the stress (5), the strain (6) and the strain rate (7) versus time within the specimen can be evaluated as:

$$\sigma(t) = E_0 \cdot \frac{A_0}{A} \cdot \epsilon_T(t), \tag{5}$$

$$\epsilon(t) = -\frac{2C_0}{L} \int_0^t \epsilon_R(t), \tag{6}$$

$$\dot{\epsilon}(t) = -\frac{2C_0}{L} \cdot \epsilon_R(t), \tag{7}$$

where E_0 is the Young's modulus of the bars, A_0 is the cross section of the input and output bars, A is the cross section of the specimen within the gauge length L, C_0 is the bar elastic wave speed, ϵ_T and ϵ_R are the transmitted and reflected pulses, respectively.

5.2 Experimental set-up for high temperature dynamic testing

The dynamic tests at high temperature were performed by means of Ambrell compact EASYHEAT induction water-cooled heating system. With reference to Figure 4, where it is depicted the set-up for the high strain rate tests at elevated temperature: input ① and the output bars ②; specimen ③; heating system ④; water-cooled induction coil ⑤; thermal controller ⑥; cooling system ⑦ for the input and output bars. The cooling systems avoid the temperature influences on the strain-gauges in input and output bars ⑧ that are sufficiently far from the heating source.

The stress and strain rate as a function of time were evaluated by using (5) and (7). The strain rate was evaluated from the proof stress till the ultimate tensile strength. The strain rate stays constant in the plastic hardening zone.

By using the heating systems, the specimen was heated with a constant heating rate of 2.78 °C/s till the target temperature. In order to obtain a homogeneous distribution along the gauge length the temperature in the specimen was kept constant

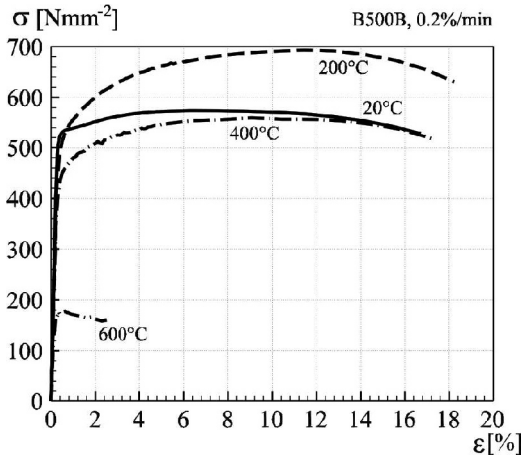

Fig. 5. Quasi-static stress versus strain curves at different temperatures.

for at least 10 min [4]. By reaching these conditions, the dynamic test was performed in steady-state conditions with the well-known procedure [22].

In order to understand the effect of the temperature on the dynamic mechanical properties of the B500B reinforcing steel, the same testing conditions adopted at room temperature were used. With these testing conditions and at 20 °C, the target strain rates were $250\,s^{-1}$, $400\,s^{-1}$ and $800\,s^{-1}$.

Three temperature were considered: 200 °C, 400 °C and 600 °C. Three tests for each testing condition and temperature were performed.

6 Experimental results

6.1 Quasi-static test results at elevated temperature

The main results of the quasi-static tests obtained at 200 °C, 400 °C, 600 °C, are shown in Tables 1 and 2.

The quasi-static stress versus strain curves at different temperature are shown in Figure 5. This graph does not show the stress-strain curves until failure of the specimens. The curves are just given until the extensometer was removed. Therefore, the curves allow to draw conclusions only with regard to the proof strength and elastic modulus and not with regard to ductility and ultimate strain.

The reduction factor for the materials properties of reinforcing steel commonly used for fire design are related to modulus of elasticity at temperature E_0, to proof strength $f_{p_0.2\%}$, and to ultimate tensile strength f_u. Figure 6 compares the temperature-dependent reduction factor for the modulus of elasticity obtained from the tests to the related value proposed by Model Code 2010 [19]. The elastic modulus of the tests are relatively higher that those recommended for design purposes.

6.2 Dynamic results at high strain rate at room temperature

The representative engineering stress versus engineering strain curves for different strain rate at room temperature are compared in Figure 7b. The strain rate causes in the material an enhancement of the strength and strain capacity as well as of the

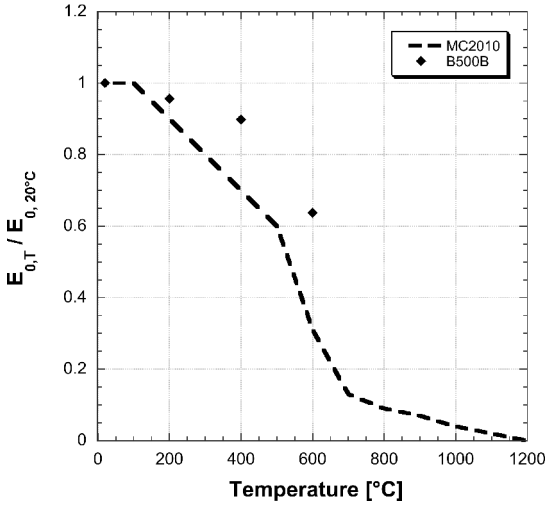

Fig. 6. Reduction factor for the elastic modulus.

Table 1. Material properties of reinforcing steel at room and high temperatures in quasi-static regime, $\dot{\epsilon} = 0.2\%/\text{min}$ (33×10^{-6} s^{-1}).

	Temperature, θ (°C)			
	20	200	400	600
Modulus of elasticity at strain 0%, E_0 (MPa)	199′600	190′900	179′200	127′200
Modulus of elasticity at strain 2%, $E_{2.0}$ (MPa)	154′600	167′700	157′600	113′600
Strain at proportional limit, ϵ_p (%)	0.215	0.177	0.162	0.068
Stress at proportional limit, f_p (MPa)	430	338	290	86
Strain at 0.2%-proof stress, $\epsilon_{p,0.2\%}$ (%)	0.465	0.465	0.445	0.339
Proof strength, $f_{p,0.2\%}$ (MPa)	530	506	440	177
Strain at ultimate strength, ϵ_u (%)	7.008	11.517	8.892	0.710
Ultimate tensile strength, f_u (MPa)	575	695	563	179

Table 2. Material properties of reinforcing steel at high temperatures in quasi-static regime, $\dot{\epsilon} = 1.0\%/\text{min}$ (167×10^{-6} s^{-1}).

	Temperature, θ (°C)		
	200	400	600
Modulus of elasticity at strain 0%, E_0 (MPa)	189′400	180′100	135′400
Modulus of elasticity at strain 2%, $E_{2.0}$ (MPa)	169′400	156′600	117′900
Strain at proportional limit, ϵ_p (%)	0.190	0.166	0.078
Stress at proportional limit, f_p (MPa)	359	300	106
Strain at 0.2%-proof stress, $\epsilon_{p,0.2\%}$ (%)	0.475	0.439	0.353
Proof strength, $f_{p,0.2\%}$ (MPa)	522	433	208
Strain at ultimate strength, ϵ_u (%)	8.514	12.268	0.499
Ultimate tensile strength, f_u (MPa)	682	570	213

plastic energy dissipation. It can be observed how the ultimate tensile strength as well as the uniform strain increase with increasing of strain rate. The Dynamic Increase Factor (DIF) for the ultimate tensile strength as a function of the strain rate is shown in Figure 7a where the results in [21,22,24] are reported.

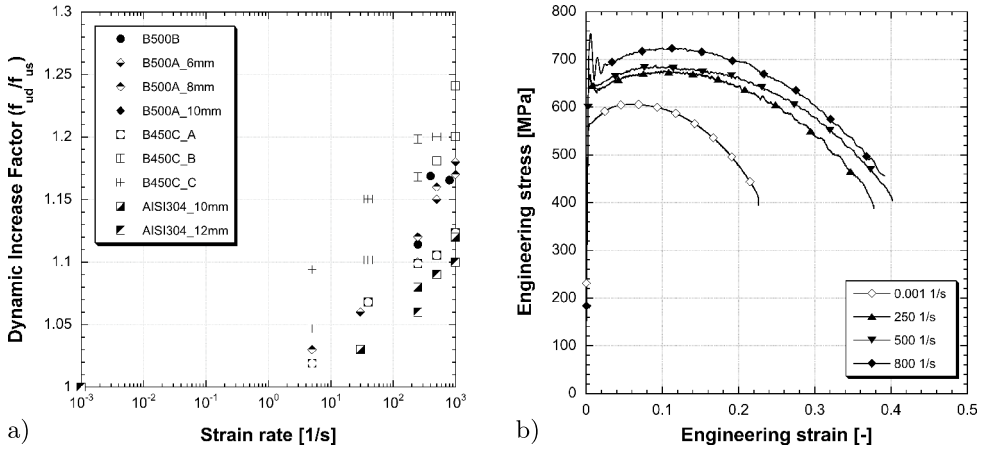

Fig. 7. (a) Dynamic Increase Factor (DIF) of ultimate tensile strength versus strain rate. (b) Engineering stress-strain curves at different strain rates and room temperature.

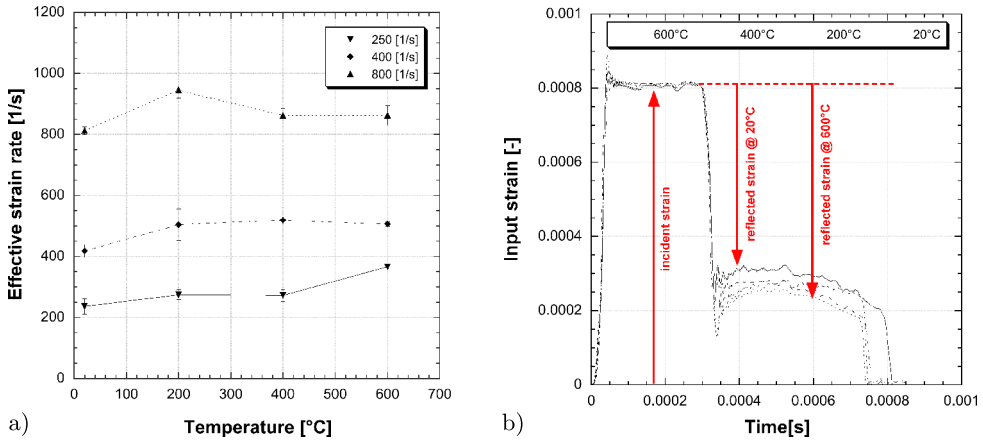

Fig. 8. (a) Effective strain rate versus temperature curves. (b) Comparison between reflected pulses at increasing temperatures.

6.3 Dynamic results with combination of high temperature and high strain rate

The experimental results obtained by the dynamic tests are collected in Tables 3, 4, and 5. The evolution of the different mechanical parameters under extreme conditions (temperature and high strain rate) is usually analysed by a comparison with the data obtained at room temperature as reference. High temperature cause a decrease of the elastic modulus causing the increase of the growth rate of the strain as well as the sound speed in the material, as result the effective strain rate increases with increasing the temperature as shown in Figure 8a. This effect can be also observed in Figure 8b as an increase of the reflected pulses for the four testing temperatures that is directly correlated with the strain rate (see Eq. (7)).

The influence of the temperature on the mechanical properties of B500B steel can be represented by depicting the engineering stress versus the engineering strain diagrams. Figure 9a shows a representative test for each temperature. It is possible to observe how the temperature reduces the ultimate tensile strength and energy absorbed in the plastic deformation.

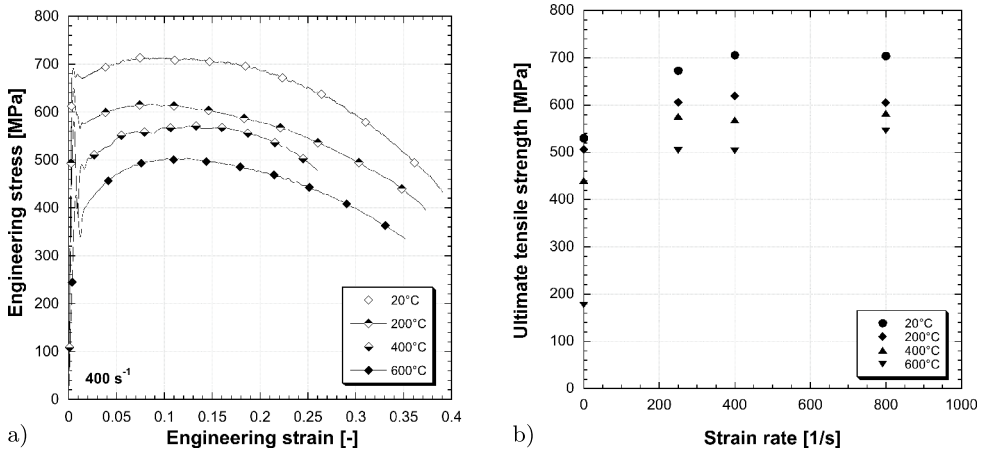

Fig. 9. (a) Comparison between engineering stress-strain curves at different temperatures. (b) Evolution of the ultimate tensile strength at different temperatures with increasing strain rate.

In Figure 9b, the evolution of the ultimate strength with increasing temperature and strain rate is depicted. It can be observed how the strain rate and the temperature act in opposite direction. On the one hand the strain rate causes an enhancement of the strength capacity, on the other hand the temperature causes a thermal softening reducing them. During the dynamic tests at high strain rate the material response showed an initial instability in the form of upper and lower yield stresses (visible in Fig. 9a), the averaged values are reported in Tables 3, 4 and 5. The upper yield stress occurs because of the dislocation density and velocity [35]. Early studies on upper yield stress were made by Campbell and Harding [36–39]. These works explained this instability with the delay time and thermal activation theory. Upper yield stress occurs because of loading rate and shear band thermal activation [38]. Harding [39] introduced a linear relation between the upper yield stress and loading rate. With the reference to the three different testing conditions (kept constant at different temperatures), the measured elastic stress rate $\dot{\sigma}$ is significantly influenced by the temperature. Increasing the temperature, the local movements of the dislocations are facilitated. Moreover, during the high strain rate tests, because of the adiabatic character of high rate deformation processes, the material undergoes a further temperature increase. This, even if limited to few dozens of degree, contributes to reduce the elastic stress rate. For example, in the case of highest velocity (800 s^{-1}), the elastic stress rate was reduced from $\dot{\sigma}_{20°C} = 41.1$ TPa/s to $\dot{\sigma}_{600°C} = 18.8$ TPa/s. At 600 °C the values of $\dot{\sigma}$ slightly varied (with an increment less than 10%) from the 250 s^{-1} to 800 s^{-1}, while at room temperature it is most significant, up to 285%.

The reduction factors for ultimate tensile strength (determined as the ratio of the value at elevated temperatures to the corresponding value at room temperature) are shown in Figure 10a, where data at the same testing condition are compared. It is possible to observe how for the quasi static tests, except for the one at 200 °C, the reduction factors seem to agree with the indication given by the Model Code [19]. At high strain rate the measured reduction factors are lower than those indicated in [19] while for the highest velocity the values proposed are more conservative. Indeed, the reduction factors proposed for the quasi-static conditions [19] are not applicable for the dynamic regimes. In any case, these results could be useful for an estimation of the reduction factor at high strain rates.

Table 3. Experimental results with a target strain rate of $250\,s^{-1}$ at 20 °C.

	Temperature, T (°C)			
	20	200	400	600
Upper yield strength, $f_{y,upper}$ (MPa)	659 ± 45	594 ± 16	492 ± 9	415 ± 15
Lower yield strength, $f_{y,lower}$ (MPa)	625 ± 41	583 ± 19	478 ± 6	371 ± 8
Proof strength, $f_{p,0.2\%}$ (MPa)	614 ± 40	554 ± 14	448 ± 8	364 ± 5
Ultimate tensile strength, f_u (MPa)	673 ± 41	606 ± 14	576 ± 17	504 ± 4
Uniform strain, ϵ_u (%)	10.9 ± 0.7	7.5 ± 0.5	13.6 ± 0.4	12.1 ± 0.7
Engineering fracture strength, f_f (MPa)	395 ± 26	386 ± 6	485 ± 21	330 ± 4
Engineering fracture strain, ϵ_f (%)	39.3 ± 2.8	36.7 ± 0.9	23.6 ± 0.4	38.7 ± 2.6
Modulus of toughness, U_t (MJ/m^3)	237 ± 31	200 ± 7	128 ± 2	175 ± 1
Reduction of cross-section area, Z (%)	65.2 ± 0.8	64.3 ± 0.5	47.3 ± 1.9	53.9 ± 0.3
True fracture strength, $f_{f,true}$ (MPa)	937 ± 64	905 ± 10	823 ± 10	652 ± 7
True fracture strain, $\epsilon_{f,true}$ (–)	1.054 ± 0.022	1.031 ± 0.013	0.64 ± 0.037	0.775 ± 0.006
Elastic stress rate, $\dot{\sigma}$(TPa/s)	14.4 ± 2.7	13.8 ± 1.4	18.6 ± 4.5	17.3 ± 0.9
Plastic strain rate, $\dot{\epsilon}$ (s^{-1})	236 ± 25	274 ± 16	272 ± 19	366 ± 7

In reinforced concrete structures the ductility of rebars have considerable importance as well as their variation at high temperatures. Different ductility indices can be considered as the ratio between the ultimate tensile strength (f_u) and the proof strength ($f_{p,0.2\%}$) or the reduction of the cross-section area at fracture (Z). The reduction of the cross-section area at fracture was computed on broken specimens with the following equation:

$$Z = \frac{A_i - A_f}{A_i}, \tag{8}$$

where A_i and A_f are the initial and final cross-section area, respectively. Furthermore, these data were used for the evaluation of the true stress-strain diagram (Fig. 10b) by using the Bridgman formulae [40], which introduce the correction for the triaxial stress state:

$$f_{f,true} = \frac{f_f}{(1 + \frac{R}{a}) \cdot \ln(1 + \frac{a}{R})}, \tag{9}$$

$$\epsilon_{f,true} = 2 \cdot \ln \frac{r}{a}, \tag{10}$$

Table 4. Experimental results with a target strain rate of $400\,s^{-1}$ at 20 °C.

	Temperature, T (°C)			
	20	200	400	600
Upper yield strength, $f_{y,upper}$ (MPa)	687 ± 18	635 ± 7	547 ± 25	415 ± 7
Lower yield strength, $f_{y,lower}$ (MPa)	622 ± 16	587 ± 23	468 ± 23	393 ± 12
Proof strength, $f_{p,0.2\%}$ (MPa)	684 ± 18	559 ± 3	463 ± 5	370 ± 12
Ultimate tensile strength, f_u (MPa)	706 ± 16	619 ± 2	569 ± 12	503 ± 17
Uniform strain, ϵ_u (%)	9.2 ± 0.8	9.1 ± 0.9	13.8 ± 1.2	11.3 ± 1.7
Engineering fracture strength, f_f (MPa)	426 ± 21	388 ± 13	479 ± 8	326 ± 25
Engineering fracture strain, ϵ_f (%)	39.2 ± 0.9	39.2 ± 4.7	27.8 ± 2.2	35.3 ± 1.2
Modulus of toughness, U_t (MJ/m^3)	249 ± 2	217 ± 24	149 ± 13	158 ± 1
Reduction of cross-section area, Z (%)	65.4 ± 1.4	65.1 ± 1.8	48.2 ± 3.2	56.0 ± 1.9
True fracture strength, $f_{f,true}$ (MPa)	1020 ± 20	924 ± 31	819 ± 24	668 ± 22
True fracture strain, $\epsilon_{f,true}$ (–)	1.062 ± 0.04	1.056 ± 0.052	0.659 ± 0.061	0.821 ± 0.043
Elastic stress rate, $\dot{\sigma}$ (TPa/s)	17.7 ± 1.6	26.5 ± 2.0	27.6 ± 2.0	17.3 ± 1.1
Plastic strain rate, $\dot{\epsilon}$ (s^{-1})	418 ± 21	504 ± 51	519 ± 42	506 ± 7

where a is the minimum radius at the reduced cross-section of the specimen, R is the meridional profile curvature radius at the reduced cross-section of the specimen, and $2r$ and $2a$ are the initial diameter and the diameter of the reduced cross-section of the specimen, respectively. These geometrical properties were obtained by means of a post-mortem examination of each specimen by using a Zeiss stereo microscope Stemi 2000.

The ratio between the ultimate tensile strength (f_u) and the proof strength ($f_{p,0.2\%}$) as a function of the temperature is shown in Figure 11a, where the marked increase of the ratio at high temperature is visible. The proof strength ($f_{p,0.2\%}$) was evaluated by extrapolating the plastic behaviour in order to avoid considering the yield instabilities.

The mechanical energy consumed by the material during straining to a failure was considered to evaluate the effect of the temperature at high strain rate. It was evaluated as follows:

$$U(T) = \int_0^{\epsilon^*} \sigma(\epsilon, T) d\epsilon, \tag{11}$$

where the value of ϵ^* was chosen to get the measure of the modulus of toughness evaluated up to the true fracture strain ($\epsilon^* = \epsilon_{f,true}$).

In Figure 11b the modulus of toughness in function of the testing conditions is reported. It is possible to observe a marked decrease up to 400 °C, while an almost constant behaviour with approximately 50% of the modulus of toughness evaluated at room temperature is noted at the higher temperatures. In Table 6 the values of

Table 5. Experimental results with a target strain rate of $800\,\mathrm{s}^{-1}$ at 20 °C.

	Temperature, T (°C)			
	20	200	400	600
Upper yield strength, $f_{y,upper}$ (MPa)	747 ± 30	681 ± 30	502 ± 34	440 ± 8
Lower yield strength, $f_{y,lower}$ (MPa)	635 ± 28	561 ± 8	460 ± 16	419 ± 3
Proof strength, $f_{p,0.2\%}$ (MPa)	644 ± 26	552 ± 18	424 ± 3	391 ± 10
Ultimate tensile strength, f_u (MPa)	704 ± 26	605 ± 16	583 ± 8	546 ± 8
Uniform strain, ϵ_u (%)	10.3 ± 0.9	9.0 ± 0.3	14.5 ± 1.7	11.6 ± 1.6
Engineering fracture strength, f_f (MPa)	421 ± 34	366 ± 19	489 ± 3	373 ± 10
Engineering fracture strain, ϵ_f (%)	38.9 ± 1.0	40.5 ± 1.9	29.8 ± 2.6	30.9 ± 4.2
Modulus of toughness, U_t ($\mathrm{MJ/m^3}$)	245 ± 26	219 ± 10	162 ± 13	152 ± 21
Reduction of cross-section area, Z (%)	66.0 ± 1.5	66.7 ± 0.4	45.9 ± 1.3	53.9 ± 1.2
True fracture strength, $f_{f,true}$ (MPa)	1014 ± 44	925 ± 46	823 ± 19	714 ± 19
True fracture strain, $\epsilon_{f,true}$ (–)	1.079 ± 0.045	1.099 ± 0.013	0.616 ± 0.025	0.775 ± 0.026
Elastic stress rate, $\dot{\sigma}$ (TPa/s)	41.1 ± 5.9	34.9 ± 6.1	25.7 ± 5.6	18.8 ± 3.4
Plastic strain rate, $\dot{\epsilon}$ (s^{-1})	812 ± 13	945 ± 26	862 ± 24	799 ± 111

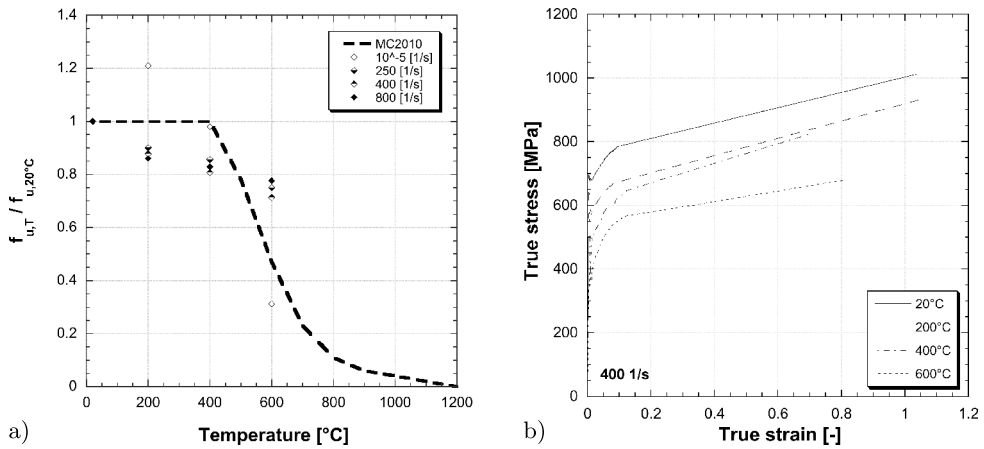

Fig. 10. (a) Comparison between reduction factors at increasing temperatures for ultimate tensile strength at different strain rate and MC2010. (b) Comparison between true stress-strain curves at different temperatures.

tensile flow stress (defined as the true stress necessary to continue deformation at any stage of plastic strain) are reported for various plastic strain, strain rate and temperature. From this table it is possible determine the strain hardening rate θ, defined as the first derivative of the flow stress σ versus true plastic strain ϵ for a given strain rate and temperature as:

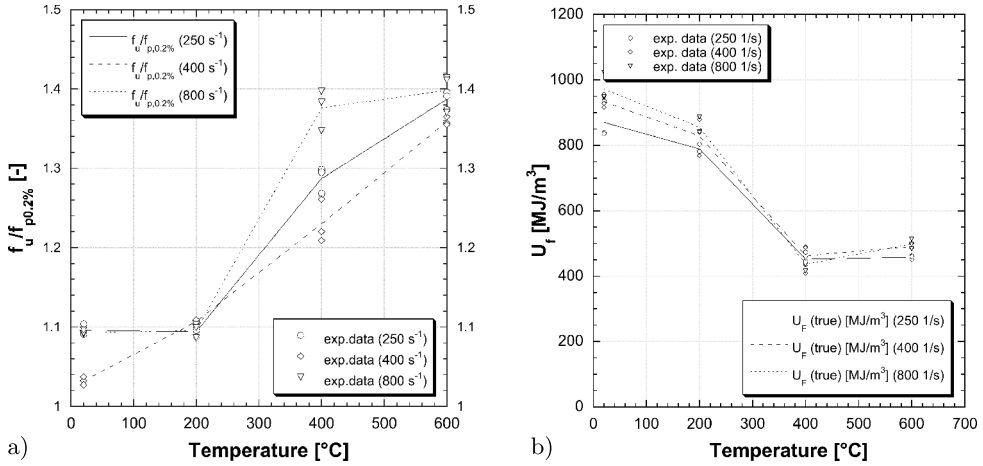

Fig. 11. Evolution of the (a) ratio between the ultimate tensile strength and the proof stress and (b) modulus of toughness in function of temperatures.

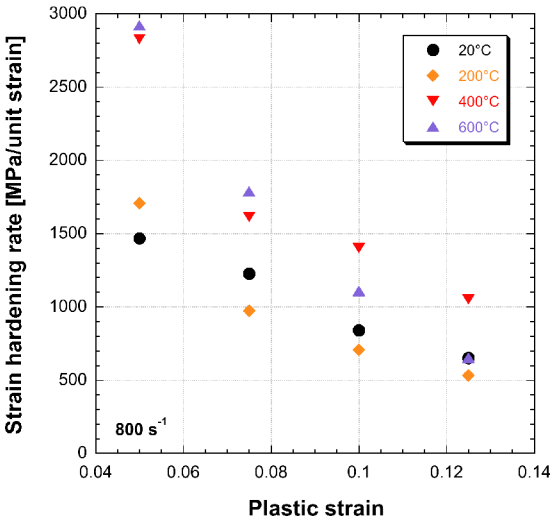

Fig. 12. Strain hardening rate @ 800 s^{-1}.

$$\theta_n = \left(\frac{\partial \sigma}{\partial \epsilon}\right)_{\dot{\epsilon},T} = \frac{\sigma_n - \sigma_{n-1}}{\epsilon_n - \epsilon_{n-1}}, \tag{12}$$

where σ_n and ϵ_n are measured tensile flow stress and corresponding plastic strain at point n, respectively. At the early stages of the plastic deformation process during a dynamic test, the strain hardening rate reaches the largest value. Subsequently, it decreases exponentially as the strain increases. The initial stress rate and the temperature affect the strain hardening rate. In Figure 12 the strain hardening rate at 800 s^{-1} is shown for the four temperatures.

Table 6. Tensile flow stress at various strain, strain rate and temperature.

Strain	T (°C)	Strain rate		
		250 s^{-1}	400 s^{-1}	800 s^{-1}
0.025	20	651	691	687
	200	597	600	583
	400	518	507	484
	600	427	433	453
0.050	20	691	727	724
	200	632	638	625
	400	577	567	555
	600	488	494	526
0.075	20	718	757	754
	200	652	662	650
	400	610	592	595
	600	529	532	571
0.100	20	742	776	775
	200	666	680	667
	400	631	620	630
	600	552	553	599
0.125	20	759	793	792
	200	677	690	681
	400	650	642	657
	600	569	566	615

7 Material constitutive relationships

7.1 Johnson-Cook constitutive law

The constitutive model proposed by Johnson and Cook (1985) [41] is commonly implemented in finite element programs due to its simplicity and easy-to-use. It is based on three phenomena, such as isotropic hardening, strain rate hardening and thermal softening. The flow stress can be expressed as:

$$\sigma = (A + B \cdot \epsilon_p^n) \cdot (1 + C \cdot \ln \frac{\dot{\epsilon}}{\dot{\epsilon}_0}) \cdot (1 - T^{*m}), \tag{13}$$

where, ϵ_p is the true plastic strain, $\dot{\epsilon}$ is the considered strain rate, $\dot{\epsilon}_0$ is the reference strain rate (taken as 1 s^{-1}) and T^* is a dimensionless temperature, valid for $T_r \leq T \leq T_m$ and defined as:

$$T^* = \frac{T - T_r}{T_m - T_r}, \tag{14}$$

where, T is the current temperature, T_m is the melting temperature and T_r is the reference temperature. T^* is equal to zero for $T < T_r$, while T^* is equal to 1 for $T > T_m$.

The parameters that can be found by means of the experimental data are A, B and n, representing the strain hardening effects of the material in quasi-static conditions, C and m representing the strain rate and the thermal softening sensitivity,

Table 7. Values of m parameters.

Temperature	Strain rate		
	250 s^{-1}	400 s^{-1}	800 s^{-1}
200 °C	1.1018	1.1042	0.9194
400 °C	1.2568	1.1803	0.9933
600 °C	1.3064	1.2723	1.3528

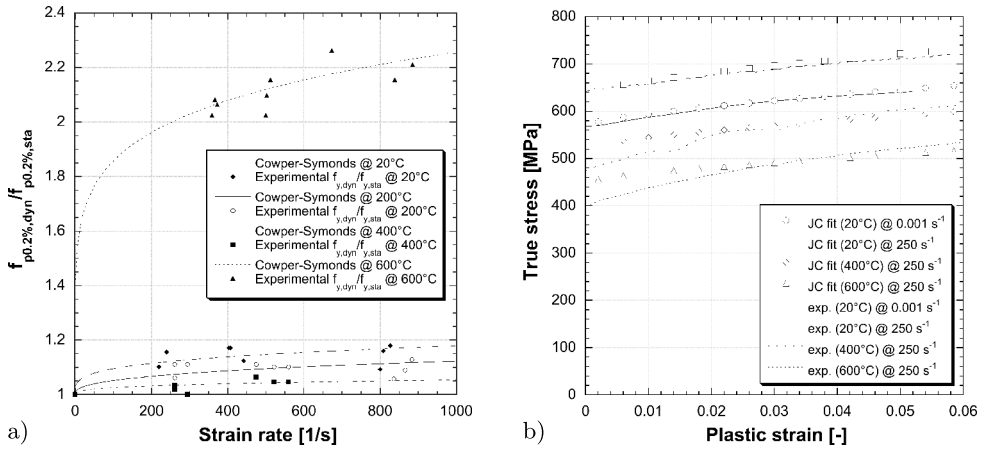

Fig. 13. (a) Comparison between the Cowper-Symonds fit and experimental results at different temperature. (b) Comparison between the Johnson-Cook fit and experimental results for 250 s^{-1} at different temperatures.

respectively. The parameters were $A = 571$ MPa; $B = 643$ MPa; $n = 0.720$; $C = 0.02143$.

The thermal softening parameter m was evaluated for three predetermined strain rates (tests at different temperatures and with comparable effective strain rate of 250 s^{-1}, 400 s^{-1} and 800 s^{-1} were used). Even if this parameter is strain rate independent in the original Johnson-Cook constitutive law, the dependency of m on both strain rate and temperature is evaluated.

In Table 7, the variation of the thermal softening parameter is shown at different strain rates as a function of temperature. It is possible to observe a noticeable variation at different temperatures, ranging from $m \approx 0.92$ to $m \approx 1.35$.

In case of combination of high dynamic loading and high temperature the effects have to be carefully evaluated. The use of a single averaged value of m in the Johnson-Cook relationship is not recommended because it could lead to significant errors, due to the high variation of the thermal softening.

Figure 13a shows a comparison between the experimental data and the values obtained by applying (13).

7.2 Cowper-Symonds constitutive law

The well-known Cowper-Symonds constitutive law [42] can be written as:

$$\frac{f_{yd}}{f_{ys}} = 1 + \left[\frac{\dot{\epsilon}}{D}\right]^{\left(\frac{1}{q}\right)}, \tag{15}$$

Table 8. Cowper-Symonds parameters.

	20 °C	200 °C	400 °C	600 °C
D	537670	249696	8219336	255
q	3.64	2.63	3.08	6.00

where f_{yd} is the true dynamic yield stress, f_{ys} is the quasi static true yield stress ($\dot{\epsilon} = 0.001\ s^{-1}$), $\dot{\epsilon}$ is the strain rate, D and q are material parameters given in Table 8. The experimental data points are fitted with the predicted curve in Figure 13b.

8 Discussions

The mechanical response of B500B reinforcing steel in tension is affected by both strain rate and elevated temperature. Testing results show that a high strain rate leads to:

- a marked initial yielding instability with upper and lower stress of the flow curve at high strain rate;
- a moderate increase of the stress at a given strain when the increasing the strain rate from 250 to 400 s^{-1};
- a modest strain rate sensitivity of the ultimate tensile strength;
- a small strain rate sensitivity of the ultimate and fracture strain;
- a small reduction of the cross-sectional area at fracture.

The behaviour at high strain rate and room temperature of this reinforced steel is in line to the other types of steel [3,21,22,24] as shown in Figure 7a.

The results further show that a high strain rate superimposed with elevated temperature leads to:

- a reduction of the initial yielding instability up to 600 °C where the same upper yield values at different strain rate are reached;
- a decrease of the flow stress with increasing temperature
- a homogenization of the elastic stress rate value at high temperature;
- a slight increase of the effective plastic strain rate with increasing temperature;
- a rapid decrease of the modulus of toughness up to 400 °C and it remains almost constant at higher temperature;
- an increase of the strain hardening rate with increasing temperature and strain rate.

The obtained results are important because the material behaviour of reinforcing steel can affect the ductility of reinforced concrete structures. In fact, the decrease of the ductility parameters, as true fracture strain or the ratio between proof stress and ultimate tensile stress, can leads to a decrease in the deformation capacity of the structural element and consequently reduce its robustness under extreme loading conditions.

The experimental results have been used to calibrate the material parameter of the B500B steel in two material constitutive relationships such as Johnson-Cook and

Cowper-Symonds. In the first constitutive relationship was highlighted a perceptible variation of the thermal softening parameter, ranging from $m \approx 0.92$ to $m \approx 1.35$. This parameter is highly influenced by the temperature and the strain rate. This leads to the conclusion that if a coupled effect of temperature and dynamic loading is considered, the use of a single averaged value of m could lead to significant errors. For these reasons different m values are proposed as a function of temperature and strain rate. The material parameters have been used to compare the Johnson-Cook previsions with the experimental data. Moreover, the Johnson-Cook parameters obtained for B500B steel are similar to those obtained by [12] on Chinese steel of same class but they were limited to maximum strain rate of 75 s^{-1} and not dependent to the temperature. Finally, the Cowper-Symonds constitutive relationship has been calibrated and compared with the experiments.

9 Conclusions

In this study, high strain rate and high temperature tests have been performed on B500B reinforcing steel in order to investigate its tensile behaviour under combined effects of fire and blast loading. First, the effects of the temperature have been studied by means of steady state tensile quasi-static test at 200°C, 400°C and 600 °C at two different low strain rates. The effects of strain rate have been also investigated at room temperature by measuring its response over a wide range of strain rate. Finally, the combination of high temperature and high strain rate have been analysed by using a Split Hopkinson Tensile Bar equipped with a water-cooled induction heating system. The main mechanical tensile property data have been reported showing that the B500B reinforcing steel is sensitive to both strain rate and temperature.

The reduction factors proposed by Model Code for the elastic modulus and for ultimate tensile strength have been compared with the experimental results obtained showing a good applicability of the Model Code provisions.

The material parameters of the two material constitutive relationships (Johnson-Cook and Cowper-Symonds) have been used to compare their previsions with the experimental data, leading to the conclusion that if a coupled effect of temperature and dynamic loading is considered, the use of a single averaged thermal softening sensitivity term, namely m, in Johnson-Cook relationship could lead to significant errors in terms of flow plastic stress. This can seriously affect a numerical simulation in which the coupled effect of temperature and dynamic load is taken into consideration.

This work is part of the research project *Behaviour of structural steels under fire in a wide range of strain rate* funded by the State Secretariat for Education, Research and Innovation of the Swiss Confederation (project C12.0051). A special acknowledgement also goes to Matteo Dotta and Claudio Scandella for their precious collaboration in performing the dynamic and quasi-static tests, respectively. The authors are grateful to the company Stahl Gerlafingen AG for providing the materials.

References

1. M. Mirmomeni, A. Heidarpour, X.L. Zhao, C.R. Hutchinson, J.A. Packer, C. Wu, Int. J. Impact Eng. **76**, 178 (2015)
2. M. Mirmomeni, A. Heidarpour, X.L. Zhao, C.R. Hutchinson, J.A. Packer, C. Wu, Constr. Build. Mater. **122**, 760 (2016)
3. E. Cadoni, M. Dotta, D. Forni, Key Eng. **711**, 791 (2016)
4. D. Forni, B. Chiaia, E. Cadoni Mater. Des. **94**, 467 (2016)

5. D. Forni, B. Chiaia, E. Cadoni, Eng. Struct. **119**, 164 (2016)
6. D. Forni, B. Chiaia, E. Cadoni, J. Constr. Steel Res. **136**, 1 (2017)
7. V. Kumar, U.K. Sharma, B. Singh, P. Bhargava, Constr. Build. Mater. **46**, 19 (2013)
8. J.C. Dotreppe, Mater. Struct. **30**, 430 (1997)
9. Y. Cao, J. Ahlström, B. Karlsson, J. Mater. Res. Technol. **4**, 68 (2015)
10. R. Felicetti, P.G. Gambarova, A. Meda, Constr. Build. Mater. **23**, 3546 (2009)
11. L.M. Dougherty, E.K. Cerreta, G.T. Gray III, C.P. Trujillo, M.F. Lopez, K.S. Vecchio, G.J. Kusinski, Metall. Mater. Trans. **40A** (2009) 1835
12. F. Lin, Y. Dong, X. Kuang, L. Lu, Materials **9**, 1013 (2016)
13. D. Asprone, E. Cadoni, A. Prota, ACI Struct. J. **106**, 523 (2009)
14. E. Cadoni, D. Forni, EPJ Web Conf. **94**, 01004 (2015)
15. E. Cadoni, M. Dotta, D. Forni, N. Tesio, Appl. Mech. Mater. **82**, 86 (2011)
16. E. Cadoni, D. Forni, High strain rate behaviour in tension of different reinforcing steels, in *Response of structures under extreme loading*, edited by V. Kodur, N. Banthia (DEStech Publications, 2015), p. 258
17. S. Hong, T.H.-K. Kang, Struct. J. **113**, 983 (2016)
18. CEB, *Concrete structures under impact and impulsive loading* (1988)
19. FIB, *Model code for concrete structures 2010* (Wiley, 2012)
20. L.J. Malvar, ACI Mater. J. **95**, 609 (1998)
21. E. Cadoni, M. Dotta, D. Forni, N. Tesio, Mater. Struct. **48**, 1803 (2015)
22. E. Cadoni, M. Dotta, D. Forni, N. Tesio, C. Albertini, Mater. Des. **49**, 657 (2013)
23. G. Riganti, E. Cadoni, Mater. Des. **57**, 156 (2014)
24. E. Cadoni, L. Fenu, D. Forni, Constr. Build. Mater. **35**, 399 (2012)
25. T. Zhong, W. Xing-Qiang, U. Brian, J. Mater. Civ. Eng. **25**, 1306 (2015)
26. A.Y. Elghazouli, K.A. Cashell, B.A. Izzuddin, Fire Saf. J. **44**, 909 (2009)
27. EN10080, Steel for the reinforcement of concrete – weldable reinforcing steel – general, European Standard
28. ISO15630-1:2010, Steel for the reinforcement and prestressing of concrete – test methods, International Standard
29. Eurocode 2, Design of concrete structures. Part 1-1: General rules and rules for buildings (2004)
30. B. Hopkinson, Philos. Trans. R. Soc. Lond. A **213**, 437 (1914)
31. R.M. Davies, Philos. Trans. R. Soc. Lond. A **240**, 375 (1948)
32. H. Kolsky, Proc. Phys. Soc. Sect. B **62**, 676 (1949)
33. C. Albertini, M. Montagnani, Inst. Phys. Conf. Ser. **21**, 22 (1974)
34. C. Albertini, M. Montagnani, Nucl. Eng. Des. **37**, 115 (1976)
35. E. Orowan, Proc. Phys. Soc. **52**, 8 (1940)
36. K. Marsh, J. Campbell, J. Mech. Phys. Sol. **11**, 49 (1963)
37. J. Campbell, Mater. Sci. Eng. **12**, 3 (1973)
38. J.D. Campbell, W.G. Ferguson, Philos. Mag. **21**, 63 (1970)
39. J. Harding, Met. Technol. **21**, 6 (1977)
40. P. Bridgman, *Studies in large plastic flow and fracture* (McGraw-Hill, 1952)
41. G. Johnson, W. Cook, Eng. Fract. Mech. **21**, 31 (1985)
42. G.R. Cowper, P. Symonds, Strain-hardening and strain-rate effects in the impact loading of cantilever beams, Technical report No. 28, Brown University